Investigation of Cutting Responses During High-speed Machining of Ti6Al4V Alloy: Finite Element Analysis

Anas Chtioui
ISPS2I Laboratory, ENSAM
Hassan II University, 150 Nil St. Casablanca
Morocco

Aissa Ouballouch
LMPGI Laboratory, EST, Hassan II
university, Road El Jadida Km 7, Oasis
Casablanca
Morocco

Ahmed Mouchtachi
ISPS2I Laboratory, ENSAM
Hassan II University, 150 Nil St. Casablanca
Morocco

Titanium alloy is one of the most widely used materials in cutting-edge technology sectors such as aerospace. In this sector, a significant portion of the components are obtained through the machining process with tight tolerances. It is well known that machining has a considerable effect on surface integrity, which in turn influences the fatigue life of these components. This work deals with numerical investigation into the impact of cutting parameters, namely, cutting speed, depth of cut, and rake angle, on cutting responses such as chip morphology, cutting forces, and residual stress. The cutting model is simulated using the Lagrangian approach through the finite element method. The Johnson-Cook-based model implemented in ABAQUS/Explicit is used to simulate the high-speed dry-cutting process of Titanium Ti-6Al-4V alloy as a 2D orthogonal cutting. This model is validated against experimental data reported in published literature. The main findings are presented and discussed.

Keywords: *residual stress, chip morphology, cutting forces, high-speed machining, cutting parameters, Ti-6Al-4V, surface integrity.*

1. INTRODUCTION

Machining is often associated with significant thermo-mechanical stresses that may result from the metallurgical and mechanical history of the material during the machining process. These thermo-mechanical stresses, known as residual stress (RS), are generated on the surface and subsurface of the machined parts and significantly contribute to their fatigue behavior. This effect can improve or diminish the rolling fatigue life of these parts [1–5], and it depends on the nature. The presence of compressive RS has the potential to enhance fatigue life and corrosion resistance. Conversely, tensile RS tends to accelerate the initiation and propagation of micro-cracks [6–8]. Based on this fact, the effect of forecasting machining process settings on RS is of great interest.

Several studies have investigated this aspect. Wan et al. [9] suggested a theoretical approach for predicting residual stresses that occur during 3D milling proce–dures. In this study, thermal and elastoplastic loading and relaxation impacts of cutting edges are considered. Yang et al. [10] proposed a hybrid modeling metho–dology that integrates 2D finite element simulation of Ti-6Al-4V material milling with a statistical model for predicting RS levels on the machined surface. Mehner et al. [11] developed a model to predict RS depth profiles in turning of EN AW-2017 based on in-process measurements of cutting forces and temperatures. Jacobus et al. [12] provided a numerical model for forecasting RS in the surface and the subsurface of the workpiece for turning processes of the steel AISI 4340. This model encompasses thermomech-anical coupling, plastic and frictional heating, heat transfer, thermal softening, and strain hardening. Den-kena et al. [13] assessed the machining process's effect on aluminum alloy's residual stresses. Results showed an obvious impact of machining settings, namely cutting-edge geometry and tool wear, on these stresses.

Various parameters, such as cutting speed, feed rate, and tool nose radius, are known for their significant impact on the quality of machined parts [14–16]. The magnitude and profile of RS in the subsurface layer are influenced by cutting parameters, namely tool wear, tool geometry, and lubrication [17]. Chaize et al. [18] investigated the impact of lubrication modes on RS generation in the turning process of an austenitic stainless steel AISI 316L. Zhang et al.[19] developed an analytical model aimed at forecasting alterations in microstructure, micro-hardness, and RS throughout the cutting process of 304 austenitic stainless steel. Leveille et al. [20] demonstrated the significant impact of cutting edge in reaming operations on martensitic stainless steel, leading to compressive residual stresses. Tao et al. [21] studied the influence of tool edge radius on residual stresses for orthogonal dry cutting of Ti6Al4V alloy using diverse cemented carbide tools. The results show a significant influence of the tool edge radius on RS variation. Machining hard materials like titanium under severe cutting conditions (high cutting speed and dry conditions) has been a difficult task, especially due to low elastic modulus and poor thermal conductivity. Machining titanium alloy is often associated with high cutting forces and temperature increases generated in the contact area of the tool-workpiece and the chip during the cutting process; this affects surface integrity, machining stability, and tool life [22]. In another work, it was found that increasing cutting speeds leads to stress state variations close to the tooltip. As a consequence, crack propagation shifts from the tooltip to the free surface of the deformed

Received: September 2024, Accepted: October 2024
Correspondence to: Ph.D. Eng. Anas Chtioui
ISPS2I Laboratory, ENSAM Hassan II University
150 Nil St. Casablanca, Morocco
E-mail: anas.chtioui@gmail.com
doi: 10.5937/fme2404616C

chip. By way of explanation, chip morphology shifts from discontinuous to a segregated continuous morphology [23]. Many studies have been conducted to assess machining process-induced residual stresses for Ti-6Al-4V. For instance, an experimental work was carried out by Veeranaath et al. [24] using a Design of Experiments (DOE). They explored the effects of parameters such as cutting speed, feed rate, and depth of cut. Considered outcomes include cutting force, temperature, chip morphology, and RS. Outeiro et al. [25] used DOE and machine learning methods to predict RS response from the cutting conditions. Kumar Sahn et al. [26] developed a 3D FEM to forecast RS through response surface methodology (RSM). The model validation, based on experimental data, led to the conclusion that elevated cutting speed and depth of cut values are favorable to generating increased compressive RS. Abboud et al. [27] and Khandai et al. [28] carried out a FE simulation for orthogonal cutting. Obtained findings were com–pared with experimental results for validation purposes. Feed rate significantly affects RS; in other terms, they become more compressive with increasing feed rate. Cutting forces and plastic deformation had an upward trend as a function of chip load. Furthermore, Ozel et al. [29] and Meng et al. [30] used FE models based on the Arbitrary Lagrangian and Eulerian (ALE) approach for orthogonal cutting. In detail, important temperatures are found at the tool-chip interface owing to friction phenomena and machining-induced stress profiles. Hence, both compressive and tensile stress regions in the sub-surface appear [29]. The combination of the orthogonal cutting model and the orthogonal indentation model was used to forecast surface residual stresses generated during the cutting process efficiently. And Zhuang et al. [31] utilized a Coupled Eulerian-Lagran–gian (CEL) approach. In this, Ti-6Al-4V machining exhibits significant compressive RS on the machined surface. RS becomes more compressive in case a large feed rate or low cutting speed is selected. Also, a large tool edge radius can lead to a machined surface that is subjected to RS and is more compressive. Liu et al. [32] explored how tool geometry influences residual stresses in the orthogonal machining of Inconel 718. Their findings indicate that using negative rake angles and sharp edge radius tends to generate higher compressive stress on the machined surface. Increased flank wear was observed to diminish the magnitude of compressive stress in the subsurface. Zou et al. [33] proposed a hybrid model to predict residual stresses in turned Ti6Al4V. They found that increasing the rake angle raises surface tensile stress while reducing compressive stress and its depth. The corner radius has little effect on stress distribution, but a larger radius extends the compressive stress range. Higher cutting speeds increase tensile stress but decrease compressive stress, and higher feed rates significantly deepen the impact of residual stress.

In the mentioned studies, the sensitivity of the results to the types of cutting parameters is observed. However, the relationship between the relevant evaluation indicators and the nature of these effects has not been completely established; it depends on addi–tional parameters, their ranges, and the type of mac–hining process. Some of these cutting conditions, reported in the literature, have a pivotal effect and require further studies to be mastered. Moreover, there is a lack of knowledge regarding dry high-speed mac–hining of aerospace materials such as Titanium alloys. This work provides insights into the selection of the most controllable key machining parameters and their ranges, as well as their effects on cutting responses. Additionally, the residual stresses in various zones and at different depths around the machined/removed layer are further analyzed.

Hence, this paper focuses on numerical investigation of the impact of machining settings on RS variation. This latter concerns the surface and subsurface during the orthogonal machining process, while the machining parameters considered are cutting speed, depth of cut, and rake angle on RS. The used cutting model is simulated by applying the Lagrangian approach by means of the Finite Element Method (FEM). The John–son-Cook-based model is implemented in ABAQUS/ Explicit to simulate the high-speed dry machining process of Ti-6Al-4V material. 2D orthogonal cutting is considered. This model is then validated with experi–mental data reported in published literature. The fin–dings in terms of RS, cutting forces, and chip morphology are presented and discussed. In the next section, the 2D finite element model will be presented in detail, including geometry, boundary conditions, material properties, and low behavior.

2. METHODS

2.1 Finite element model

The complexity of machining modeling lies in its intricate nature, involving numerous physical phenome-na such as material deformation, heat generation, and tool wear. These phenomena are influenced by a variety of factors, including the material properties of the workpiece and the cutting tool and cutting settings (cutting speed, feed rate, depth of cut, lubrication). Our FE model simulates the physical behavior of the cutting process in a detailed and accurate manner. Among the outcomes of this model, we find elastoplastic deformation of machined material, heat flux profile in the tool and the workpiece, and formation/segmentation of chips. These outcomes are obtained based on input parameters (cutting conditions). The geometry, which encompasses the workpiece and the tool, was created by means of ABAQUS. Material properties assigned to this geometry are listed in Table 1. The Lagrangian formulation is adopted in conjunction with coupled thermo-mechanical transient analysis. The workpiece is modeled as deformable, displaying elastic-plastic characteristics throughout the machining process. Meanwhile, the cutting tool is assumed to be rigid.

Regarding the geometry shown in Figure 1, the workpiece measures 1 mm in length, 0.5 mm in height, and 2 mm in width. The cutting tool is designed with a rake angle (γ) of 0 degrees, a clearance angle of 7 degrees, and a tool nose radius of 0 mm. The machining process will be conducted under dry conditions without the application of any lubricant.

Table 1. Physical and mechanical properties of the workpiece (Ti6Al4V) and tool (W. Carbide) [34]

Properties	Density (kg/m3)	Elastic modulus (GPa)	Poisson's ratio (v)	Specific heat (J/kg□)	Thermal conductivity (W/m□)	Thermal expansion (□-1)	Melting temperature (□)
Ti6AL4V (Wp)	4430	113	0.342	546	7	9.1E-6	1630
W. Carb (Tool)	11 900	534	0.22	400	50	5	-

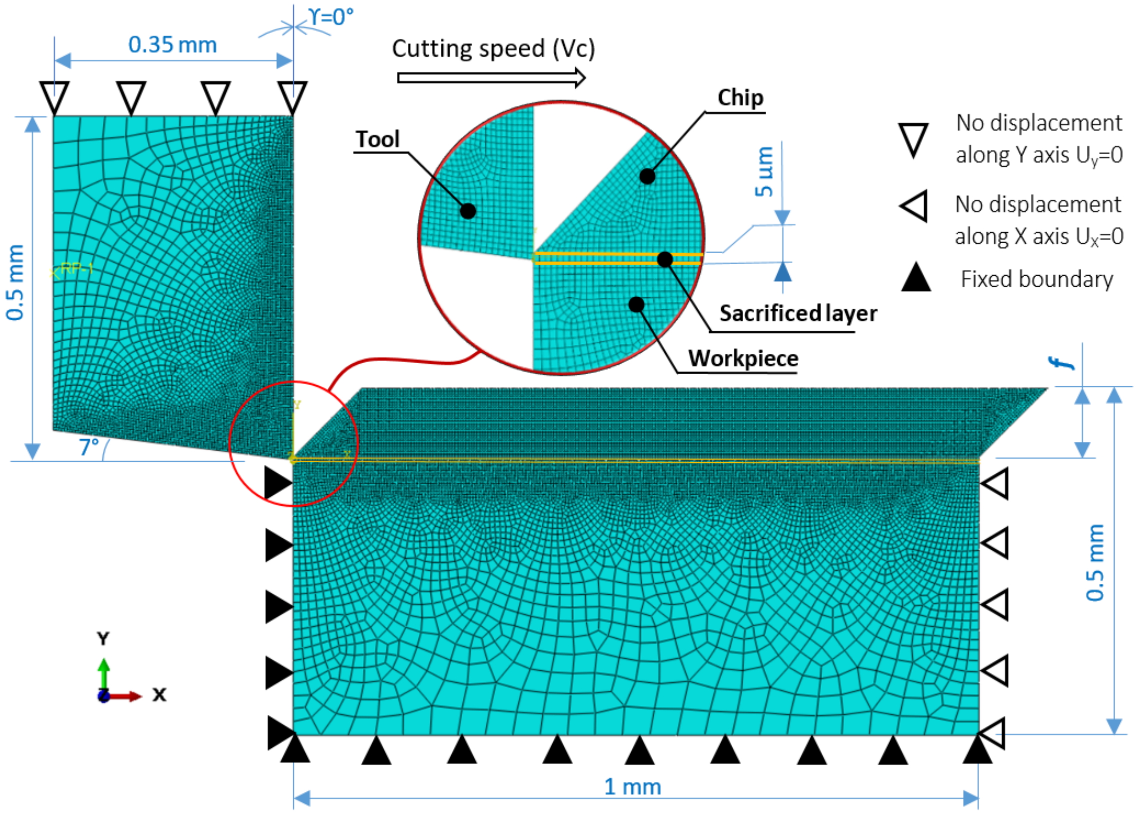

Figure 1. Model set-up and boundary conditions

Displacement in the x and y-axis of the workpiece is annulled in what concerns indicated boundaries, and a prescribed displacement is given to the tool in the x-axis positive direction at the feed 'f.' In the 2D case, 'f' refers to the feed rate and uncut chip as they express the same factor. The cutting model and the boundary conditions are illustrated in Figure 1.

The Lagrangian formulation is adopted, where the mesh tracks the material's deformation during the cutting process. Quadrilateral elements of type CPE4RT with four nodes, under plane strain conditions, are utilized to simulate geometry. A mesh grading strategy is applied to both the workpiece and the tool. To achieve a balance between precision and efficiency in the simulation, the mesh element sizes in the workpiece were defined considering the work conducted by Xu et al. [35]. The tool elements size in the tool-chip contact area is similar to that of the workpiece. According to serial simulation trials, the dimensions and direction of the workpiece elements influence the mesh convergence and highly affect the results.

The mesh size of elements was chosen to be as small as possible to ensure maximum accuracy while considering result stability and meshing convergence. The area where the machined surface layer and chip are formed is refined to 2,5 µm, while the workpiece (bottom) and the tool are meshed with element sizes ranging from 2,5 to 40 µm to ensure acceptable accuracy and computational efficiency simultaneously. The mesh is angled at 45° to facilitate segmented chip formation. An initial temperature of 20°C is assigned to the workpiece and the tool. Other fixed conditions are clearance angle and tool nose radius. These details are depicted in Figure 1. Table 2 summarizes the cutting parameters selected for our numerical simulation.

Table 2. Cutting parameters

Parameters	Values
Cutting speed (m/min)	500, 750, 1000, 1500, 2500
Feed (mm)	0.05, 0.08, 0.1
Rake angle (degree)	-6, 0, +6
Tool nose radius (mm)	0

With regard to the adopted model to simulate the machining of this workpiece is presented in detail in the next paragraph.

2.2 The constitutive model

To describe the interaction between moving parts and to represent the constitutive behavior of work materials under high-speed cutting conditions in FE modeling, the Johnson-Cook model is adopted to characterize the flow stress of material considering the effect of strain, strain rate, and temperature. The general form is as follows (1):

$$\bar{\sigma} = \left[A + B\bar{\varepsilon}^n\right]\left[1 + C\ln\left(\frac{\dot{\bar{\varepsilon}}}{\dot{\bar{\varepsilon}}_0}\right)\right]\left[1 - \left(\frac{T - T_r}{T_m - T_r}\right)^m\right] \quad (1)$$

where $\bar{\sigma}$ is the flow stress, $\boldsymbol{A}$ is the yield stress, $\boldsymbol{B}$ and $\boldsymbol{n}$ are the strain hardening parameters ($\boldsymbol{B}$ is the har–dening modulus and $\boldsymbol{n}$ is the work-hardening exponent), $\boldsymbol{C}$ is the strain-rate sensitivity coefficient, $\dot{\bar{\varepsilon}}$ is the plastic strain, $\dot{\bar{\varepsilon}}_0$ is the reference strain rate, $\boldsymbol{T_r}$ is the room temperature, and $\boldsymbol{T_m}$ is the melting temperature of the material, and m is the thermal softening exponent. The J-C model constants are summarized in Table 3.

Table 3. Constants of the J-C model for Ti6Al4V [36]

Material constant	Values
A (MPa)	782.7
B (MPa)	498.4
n	0.28
C	0.028
m	1
Tm (□)	1630
Tr (□)	25
$\dot{\varepsilon}_0$ (/s)	10-5

A damage model that considers material behavior under extreme conditions is essential to simulate the formation of serrated chips during machining accurately. The main objectives of this model are to precisely predict the initiation and propagation of cracks, the development of shear bands, and the resulting chip morphology. The damage initiation criterion in the J-C model is defined by an accumulated damage parameter w (2):

$$w = \Sigma\frac{\Delta\varepsilon}{\varepsilon_f} \quad (2)$$

where $\Delta\varepsilon$ is the increment of equivalent plastic strain, ε_f is the fracture strain at failure and is defined by (3):

$$\varepsilon_f = \left[d_1 + d_2\exp\left(d_3\frac{P}{\bar{\sigma}}\right)\right]\left[1 + d_4\ln\left(\frac{\dot{\bar{\varepsilon}}}{\dot{\bar{\varepsilon}}_0}\right)\right]\left[1 + d_5\left(\frac{T - T_r}{T_m - T_r}\right)\right] \quad (3)$$

where ε_f influenced by factors such as the non-dimen–sional equivalent plastic strain rate, the ratio of hy–dro–static pressure to the flow stress $\frac{P}{\bar{\sigma}}$, temperature, and specific damage constants d1 to d5 that depend on mec–hanical properties and are obtained through experimen–tal tests (their values for Ti6Al4V are listed in Table 4).

Fracture energy is a fundamental mechanical pro–perty that quantifies the amount of energy required to propagate a crack or fracture within a material. It rep–resents the resistance of a material to fracture and is a critical parameter in understanding its fracture behavior.

Table 4. The fracture constants of the JC fracture model for Ti6Al4V [37]

d1	d2	d3	d4	d5
-0.09	0.25	-05	0.014	3.87

When material damage occurs, such as the initiation and propagation of cracks, the stress-strain relationship cannot precisely represent the material's behavior. In this case, fracture energy becomes a crucial factor in determining the material's ability to resist fracture under applied loads. The fracture energy is given as (4):

$$G_f = \int_{\bar{\varepsilon}_0}^{\bar{\varepsilon}_f} L\sigma_y d\bar{\varepsilon} = \int_0^{\bar{u}_f} \sigma_y d\bar{u} \quad (4)$$

where $\bar{\varepsilon}_0$ is the initial plastic strain that is zero before the damage initiates, and L is the characteristic length, $\bar{u}$ is the equivalent plastic displacement as the fracture work conjugate of the yield stress after the onset of the damage (σ_y), $\bar{u}_f$ is the equivalent plastic displacement at failure. The fracture energy $\boldsymbol{G_f}$ may be deducted from the fracture toughness ***Kc*** [38] (5).

$$G_f = \left(\frac{1 - v^2}{E}\right)K_c^2 \quad (5)$$

The stiffness degradation of materials during da–mage evolution may be expressed by the variable $\boldsymbol{D}$. When $\boldsymbol{D}$ increases from 0 to 1, the entire fracture occurs given in (6):

$$D = \frac{L\bar{\varepsilon}}{\bar{u}_f} = \frac{\bar{u}}{\bar{u}_f} \quad (6)$$

where the equivalent displacement ($\bar{u} = L\bar{\varepsilon}$), and equi–valent displacement at failure $\left(\bar{u}_f = \frac{2G_f}{\sigma_{y0}}\right)$, where $\boldsymbol{\sigma_{y0}}$ is the yield stress at the damage initiation.

A combined Coulomb and shear friction models, has been employed to simulate the high pressure at the surface contact, interface the tool /the workpiece, as a result of plastic deformation during the chip removal process. They can be expressed as in (7) and (8):

$$\tau = \min\left(\tau_y, \mu\sigma\right) \quad (7)$$

$$\tau_y = \sigma / \sqrt{3} \quad (8)$$

where $\boldsymbol{\tau}$ is the frictional stress, $\boldsymbol{\sigma}$ is the normal stress, $\boldsymbol{\tau_y}$ is the yield shear stress, ***and*** $\boldsymbol{\mu}$ is the friction coefficient considered as **0.4** [31]. Also, the fraction of the heat as **0.9** and the heat generated by friction as **1** are imple–mented in the model to obtain the profile temperature during the cutting process.

After implementing the model with all input data and various constants, we will focus on the results in the following section. They are principally concerned with cutting forces, chip morphology, and residual stress.

3. RESULTS AND DISCUSSION

In this section, we start with validation elements and corresponding experimental data. Then, the results in terms of cutting parameters effect of various considered responses.

To validate this FE model, a comparison was made between numerical results and experimental measure–ments. These findings are cutting forces and chip morp–hology as a function of cutting speed, which ranges from 500 to 2500 m/min. The same conditions are considered in both studies and are similar to those stated in the literature. These conditions are shown in Table 5.

This FE model is optimized as the thickness of the sacrificed layer affected by machining was chosen to be as small as possible (5 µm). Hence, dislocations were limited, and the accuracy of the results increased following the Lagrangian approach.

Table 5. Cutting parameters for the validated model

Cutting speed (m/min)	Feed (mm)	Rake angle (°)	Clearance angle (°)	Tool nose radius (µm)
500-2500	0.1	0	7	0

In the next subsection, the results of cutting forces are presented and compared to experimental data.

3.1 Predicted cutting forces and validation

Cutting forces in machining result from several phe–nomena, primarily the plastic deformation of the work–piece material and the friction between the cutting tool and the workpiece. In regions where the force momen–tarily increases, the material may deform more plas–tically and at a faster rate, which leads to localized areas of higher temperature and strain. The fluctuations in cutting force can arise from the presence of serrated chips, indicative of uneven plastic deformation (Figure 2). These fluctuations are associated with the transfor–mation in the morphology of the chips. As can be seen from Figure 2, during machining initiation, these fluc–tuations are more important, and a difference of 283N in terms of cutting force is achieved. This phenomenon can drastically affect the fatigue behavior of the machi–ned parts. For model validation, reaction forces were compared with the results of orthogonal cutting tests conducted by Wang et al. [39] under similar cutting conditions (Table 5). This comparison is depicted in Figure 3.

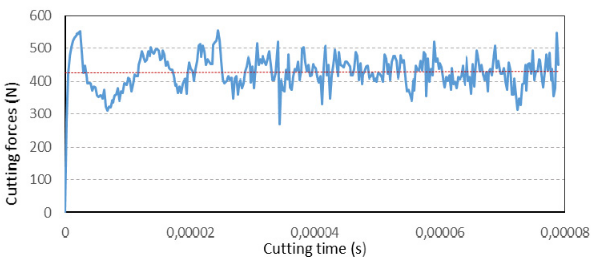

Figure 2. Simulation results of cutting forces under Vc 500 m/min cutting speed.

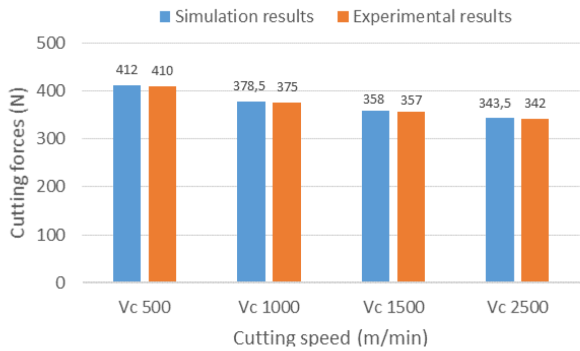

Figure 3. Cutting forces comparison in terms of cutting speeds.

Cutting forces are drawn and analyzed, altering the cutting speed from 500 to 2500 m/min. Numerical results are in agreement with experimental findings with an error of less than 1%. The results show a reduction in cutting forces of approximately 17%; this is in compli–ance with the fact that a decline in cutting force occurs with a rise in cutting speed [39–42]. The increased cut-ting speed can explain the observed pattern; this conse–quently elevates heat flux, causing material softening. Subsequently, this softening leads to a reduction in cutting forces. This behavior was also reported in pre–vious studies on AISI 4340 steel [43] and AA7075-T651 [44]. According to these findings, high cutting speeds are recommended. However, other responses should be optimized.

In addition to cutting speed impact, other machining conditions, such as feed and rake angle, affect some responses, such as chip morphology. The next subsection will detail this.

3.2 Predicted chip morphology and validation

Analyzing chip morphology is essential for under–standing the cutting process due to its significant impact on the entire machining operation. Chips encapsulate the primary mechanisms occurring in the cutting zone (Figure 4). For example, high localized deformation, abrupt temperature increases, damage and fractures, and changes in microstructure.

A comparison of chip formation mechanism bet–ween our model and the experimental study conducted by Wang et al. [39] is presented in Figure 5. It is highly affected by cutting parameters, and the effect trends are in line with the findings from the experimental work. The detailed results are illustrated in Figure 6. The characteristics of segmented chip morphology com–monly proposed in the literature, including shear angle (□), pitch (p), valley (v), and peak (H), are measured geometrically from the simulation model, as shown in Figure 4. The evolution of chip morphology under variation of cutting speeds is presented in Table 6. For quantitative characterization of serrated chips, several researchers defined the serration degree (Gs) of the chips by the following equation (9). Figure 5 illustrates the evolution of serration degree (*Gs*) as a function of cutting speed.

$$G_s = \frac{H - v}{H} \qquad (9)$$

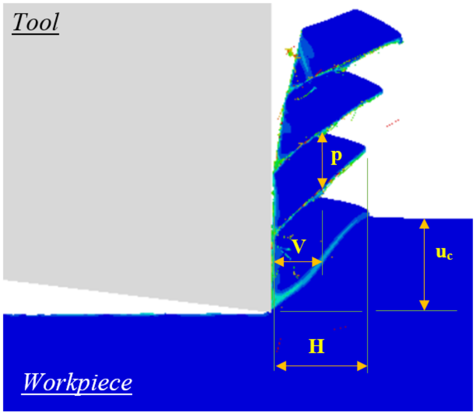

Figure 4. 2D orthogonal cutting schematic of serrated chip geometry.

Increasing cutting speed from 500 to 2500 m/min, both the peak and the valley decrease, and the pitch of shear bands space increases, as presented in Table 5. However, the shear angle and the serrated degree increase with cutting speed, which is consistent with machining theory, suggesting that when cutting speed increases, machining forces decrease (as presented in Figure 3). At a cutting speed of 2500 m/min, the degree of serration (Gs) attends to 1, indicating that adjacent segments of serrated chips are separated from the workpiece, as can be seen in Figure 6.

Table 6. Simulation results of segmented chip sizes under various cutting speeds feed 0.1mm and rake angle 0°

Vc (m/min)	Peak (µm)	Valley (µm)	Pitch (µm)	Shear angle □ (°)	Gs
500	136.4	74.9	40	36	0.45
750	132.4	57.6	44.3	37	0.56
1000	129.6	46.5	47.1	38	0.65
1500	126.2	22	47.8	39	0.83
2500	102.8	-	56.6	44	1

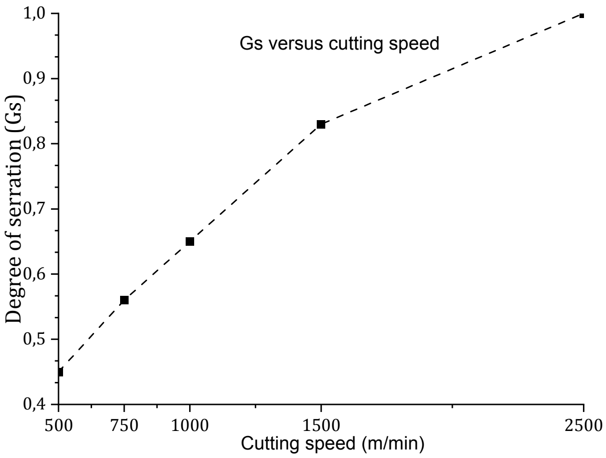

Figure 5. Evolution of serration degree (Gs) as a function of cutting speed.

Figure 6 and Figure 7 show the variation of chip geometries under cutting speeds altering from 500 to 2500 m/min, also highlighting the patterns of equivalent plastic strain (PEEQ). With constant feed and rake angles equal to 0.1 mm and 0°, respectively. As cutting speeds rise, the serration on the chips intensifies, re–sulting in a marked transformation in chip geometry. At a speed of 2500 m/min, the chip starts to separate, aligning with experimental results found by Wang et al. [39]. Feed combined with cutting speed has a very significant impact on the morphology of the chip.

In other terms, at a low feed of 0.05 mm with a lower cutting speed of 500 m/min, the chip morphology occurs, the serrated chip diminishes, and it begins to converge towards a more regular and continuous form. In contrast, as the feed increased, the chips formed were more seg–mented. For the rake angle, it has a remarkable influence on the chip morphology; a positive rake angle of 6 degrees combined with a low speed at 500 m/min and low feed at 0.05 mm generates a continuous chip. The chip becomes more segmented as the speed increases.

Sun et al. [45] examined the machining of Ti-6Al-4V and concluded that the variations in cutting forces stem from chip segmentation, particularly the peak in cyclic force attributed to this segmentation process. Su et al. [46] explored how chip segmentation impacts surface quality and observed a significant relationship between the geometric characteristics of segmented chips and the resulting surface roughness. Several studies [47–49] tend to associate microstructure changes with the formation of adiabatic shear bands during machining.

The segmented chip is characterized by periodic shear bands. These bands form zones of severe deformation localization, resulting in significant microstructural distortion in this region. Segments of low deformation separate the shear bands. An area of extremely deformed microstructure, like the shear bands, has been stated in the secondary shear zone, affecting the workpiece surface and subsurface.

In the published literature, Davis et al.[50] investigated the transition in chip morphology, observing the shift from saw-tooth (for 0.1 m/s) to continuous (for 0.5 m/s). This prompts an intricate question into alterations in the dynamic material behavior across slow and moderate cutting speed ranges, primarily influenced by shear strain and strain rate. An experimental study conducted by Cotterell et al. [51] on the machining of Ti6Al4V showed that the segmentation frequency rises linearly with elevation in cutting speed, and it declines as feed rises. Li et al. [52] worked on the formation of serrated chips during orthogonal cutting of the Ti-6Al-4V titanium alloy. They explored different rake angles and cutting speeds. The results showed that the degree of chip segmentation rises with higher cutting speed and feed rate while it decreases with an increase in rake angle. Hua and Shivpuri [53] observed a phenomenon where rising cutting speeds lead to a shift in stress distribution near the tool tip during machining. Consequently, crack propagation moved from the tooltip to the free surface of the deformed chip within the shear zone. This change in crack behavior was identified as the primary mechanism responsible for the chip transitioning from a discontinuous to a segregated continuous morphology.

Besides these effects illustrated in the above-menti–oned subsections, residual stress is a main characteristic of surface integrity and is highly dependent on cutting parameters. The following subsection presents the resi–dual stress variation versus cutting conditions conside–red in detail.

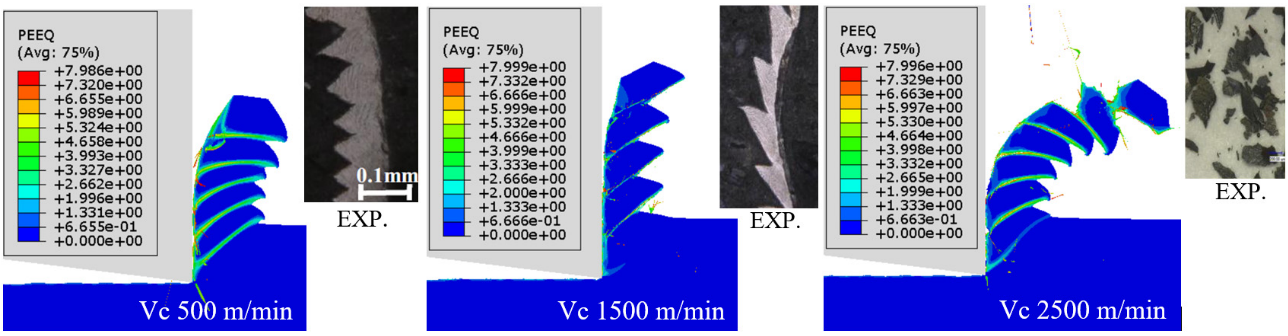

Figure 6. Comparison between predicted chips and experimental data [39]

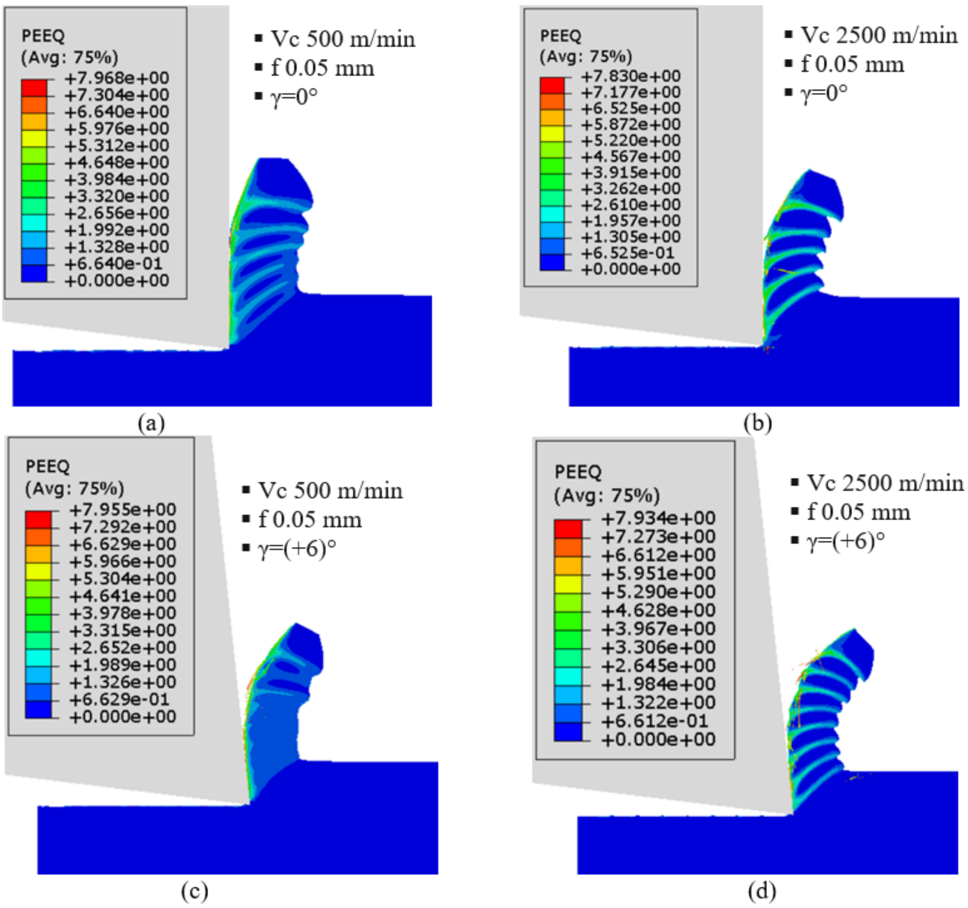

Figure 7. Summary of the effect of cutting conditions on the chip geometry.

3.3 Effect of cutting parameters on residual stress

To assess the distribution of residual stresses, it is crucial to understand the mechanisms of RS formation induced during machining. This understanding improves the relevance of simulations using Finite Element Method (FEM). Figure 8 illustrates the mechanism of RS distribution σxx in the direction of cutting speed. This distribution is strongly influenced by the interaction between the tool and the workpiece during machining, leading to the formation of four distinct zones: Zone 1 (represented in detail in Figure 9), located at the surface and subsurface layers to a depth of 20 µm. These stresses are induced by the metallurgical and mechanical history of the material during the machining operation. Indeed, they persist in the machined parts, which are not subjected to any external loads. These stresses are balanced throughout the volume and remain stored in the subsurface. It was found that they are often considered the most influential factor affecting surface integrity, making the study of this zone of great importance. As we will see later, the distribution of RS changes due to the effect of cutting parameters. In this zone, stresses vary from a state of high compression to a moderate state of tensile before converging to zero at a certain depth. Zone 2 is located below the first zone, along the direction opposite to the shear plane extension to a depth of 100 µm from the machined surface; this zone represents the extension of the shear zone. In this zone, moderate tensile stresses are generated. Zone 3 is located near and ahead of the cutting edge, where high compressive stresses are formed. Zone 4 experiences significant tensile stresses due to thermomechanical loading during the shearing of the material to form the chip, representing the periodic crack initiation model.

Regarding residual axial stress field at depth, it is observed that residual compressive stress field changes beyond a depth of 11 µm. Tensile residual stresses ap–

pear in the sub-surface (10–40 µm). The maximum of compressive RS is found at a depth of 6–10 µm. To be more exact and precise, each cutting parameter will be altered to observe its effect of residual stress profile and distribution at a position near to machined surface (path). Hence, these effects will be presented and dis–cussed below.

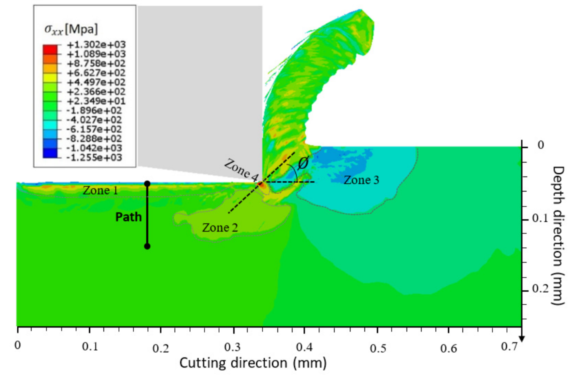

Figure 8. Mechanism of RS distribution during machining

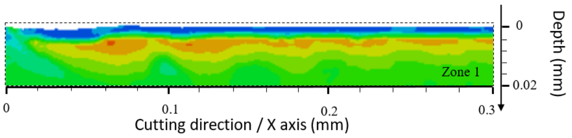

Figure 9. RS distribution in surface and subsurface (zone 1) during machining

To analyze the effect of cutting speed, RS was determined by extracting data from path 1 along the depth direction for a distance of 100 µm. Figure 10 displays the outcomes of RS profile measurements. The significant impact of cutting speed on the magnitude and distribution of residual stresses at the surface and sub-surface is illustrated. It was observed that Vc 1500 and Vc 2500 m/min exhibited notably moderate tensile stresses on the surface, whereas compressive stresses on the surface and sub-surface resulted from velocities Vc 500 and Vc 750 m/min. The analysis indicates that lower cutting speeds lead to the formation of compressive RS.

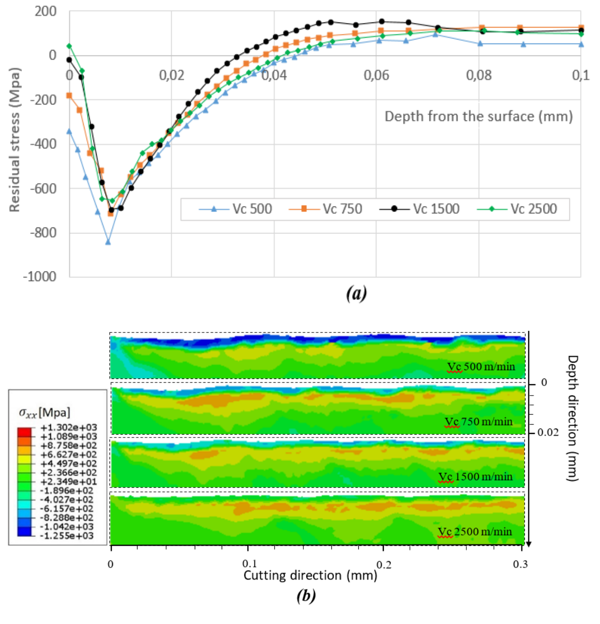

Figure 10. RS Simulation at Vc 500 to 2500 m/min, feed 0.1 mm and *γ*=0°, (a) RS profiles, (b) RS distribution

The influence of cutting speed on RS has been stu–died by several researchers [30,31,54,55]; these studies show the same effect: decreasing cutting velocity results in more compressive RS. In contrast, Sun and Guo [56] conducted a series of end milling experiments aimed at comprehensively characterizing surface integrity across a range of milling conditions. These conditions included cutting speeds ranging from 50 m/min to 110 m/min and feed from 0.06 to 0.14 mm/tooth. The findings suggest that as cutting speed increases, residual stresses tend to become more compressive. Furthermore, RS is affected by the feed. This point will be detailed in the next paragraph.

After the extraction of data from path 2 along the depth direction for a distance of 100 µm, it was noticed that the feed influences the magnitude and the state of residual stresses. Increasing the feed to 0.1 mm leads to higher compressive residual stresses while decreasing the feed to 0.05 mm results in a moderate compressive RS on the surface. This tends towards tensile RS in depth (Figure 11). These results are coherent with the study conducted by Zhuang et al. [31]. In this study, the authors investigated the effect of uncut chip thickness (ranging from 0.01 to 0.08 mm) and cutting velocity maintained at 70 m/min on the RS using inserts with two different edge radius (rε = 0.03 mm, 0.05 mm). They found that employing a larger uncut chip thickness or reducing cutting velocity tends to result in more compressive RS. Moreover, tools with larger edge radii result in greater compressive RS on the machined. Meng et al. [30] examined the impact of various uncut chip thicknesses (0.1, 0.15, 0.2, and 0.25 mm) on surface RS, with a constant cutting speed of 150 m/min. Their outcomes revealed a decrease in compressive surface RS and an increase in tensile subsurface RS as the uncut chip thickness ranged from 0.1 to 0.25 mm. The difference between the two studies clearly highlights the importance of the depth of the cut margin. For low depths, increasing the feed from 0.01 to 0.08 mm results in more compressive RS. Conversely, with larger depths of cut, rising the feed from 0.1 to 0.25 mm leads to a decrease in compressive RS.

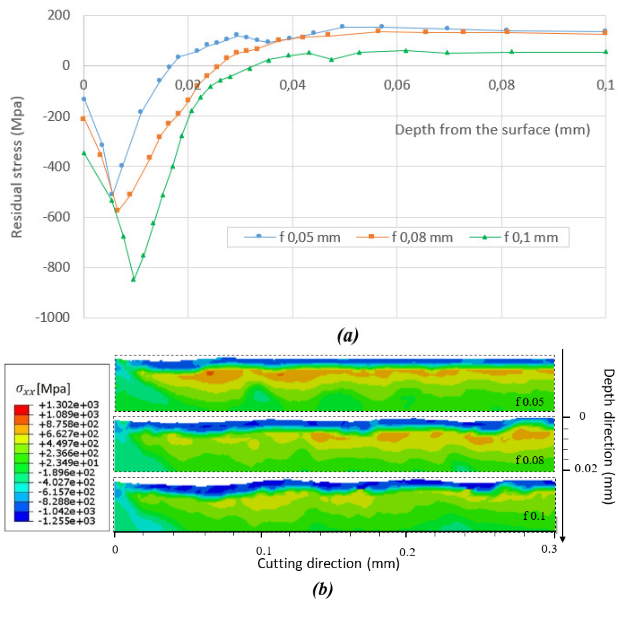

Figure 11. RS Simulation at Vc 500 m/min, *γ*=0°, feed 0.05, 0.08, and 0.1 mm, (a) RS profiles, (b) RS distribution

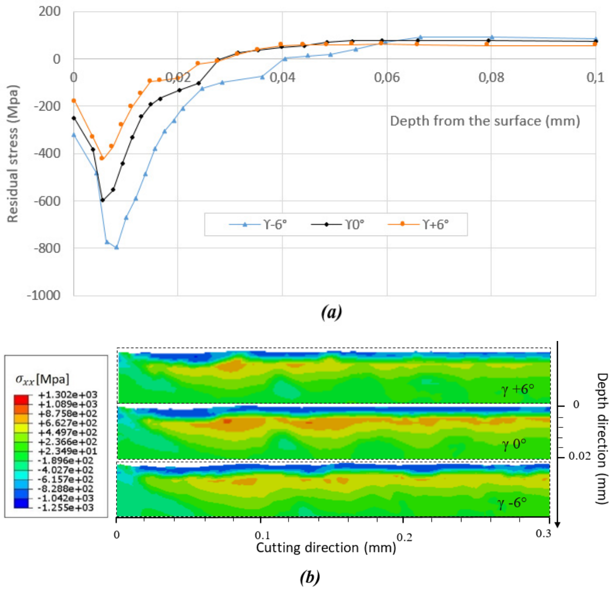

Figure 12. RS simulation at Vc 500 m/min, feed 0.05 mm, rake angle γ (+6°,0°, and -6°), (a) RS profiles, (b) RS distribution

4. CONCLUSION

In this work, finite element simulation of orthogonal cutting has been carried out for Ti6Al4V to develop a predictive tool for residual stresses. The following cut–ting parameters, cutting speed (500 to 2500 m/min), feed (0.05 to 0.1 mm), and rake angle (-6°, 0° and +6°) were considered. Their effect on RS, chip morphology and cutting forces was presented and discussed. John–son-Cook model was used in this numerical invest–igation with the Lagrangian approach. After comparing both experimental and numerical data from the lite–rature, the model was validated and served to highlight the effect of selected parameters. The results show that, regardless of the values of the mentioned parameters, the depth of the layer affected by the axial stress field does not exceed 40 µm. It is observed that residual compressive stress field changes beyond a depth of 11 µm. Tensile residual stresses appear in the subsurface (10–40 µm). The maximum compressive residual stress is found at a depth of 6–10 µm.

Besides that, the next conclusions can be drawn: Residual stresses are more compressive when the cut–ting speed is reduced to 500 m/min and become tensile as the cutting speed increases to 2500 m/min. Residual stresses become more compressive as the feed rises from 0.05 to 0.1mm. Compressive stresses have a dow–nward trend as the rake angle increases from (+6°) to (-6°). Given the impact of RS on the fatigue life of mechanical components, tensile stresses induced during high-speed machining at cutting speeds (e.g. Vc 1500 and Vc 2500 m/min) on the surface of the workpiece are unfavorable. In this case, the surfaces necessitate a super finishing process. On the other hand, lower cut–ting speeds (e.g. Vc 500 and Vc 750 m/min) positively influence fatigue life by producing a high level of compressive RS. The feed and the rake angle both have a significant impact on RS distribution. For instance, increasing the feed to 0.1 mm leads to favourable compressive RS. Similarly, a negative rake angle results in high compressive RS.

These results obtained will be useful for manufacturers and industrialists in identifying optimized cutting conditions and corresponding ranges. Hence, they will ensure machining efficiency and durability of tools, workpieces and machines. For instance, considering outcomes related to residual stress, compressive ones enhance fatigue life of machined alloys.

As a continuation of this work, our future study will tackle fatigue life of machined alloys, which is directly linked to surface integrity. The latter encompasses residual stress, surface roughness, and microstructure changes. We will assess and explore these responses in depth.

REFERENCES

[1] Weng, J.; Liu, Y.; Zhuang, K.; Xu, D.; M'Saoubi, R.; Hrechuk, A.; Zhou, J.: An analytical method for continuously predicting mechanics and residual stress in fillet surface turning. Journal of Manufacturing Processes, **68**, 1860–1879 (2021).

[2] Javidi, A.; Rieger, U.; Eichlseder, W.: The effect of machining on the surface integrity and fatigue life. International Journal of Fatigue, **30**, 2050–2055 (2008).

[3] Wang, Z.-M.; Jia, Y.-F.; Zhang, X.-C.; Fu, Y.; Zhang, C.-C.; Tu, S.-T.: Effects of Different Mechanical Surface Enhancement Techniques on Surface Integrity and Fatigue Properties of Ti-6Al-4V: A Review. Critical Reviews in Solid State and Materials Sciences, **44**, 445–469 (2019).

[4] Sasahara, H.: The effect on fatigue life of residual stress and surface hardness resulting from different cutting conditions of 0.45%C steel. International Journal of Machine Tools and Manufacture, **45**, 131–136 (2005).

[5] Welch, M.: An empirical approach to a compre–hensive damage-equivalent stress function for fatigue. FME Transactions, **50**, 535–547 (2022).

[6] Wagner, L.: Mechanical surface treatments on tita–nium, aluminum and magnesium alloys. Materials Science and Engineering: A, **263**, 210–216 (1999).

[7] Guimaraes, M. C. R.; Fogagnolo, J. B.; Paiva, J. M.; Veldhuis, S.; Diniz, A. E.: The impact of the cutting parameters and tool condition on surface integrity when milling Inconel 625. Journal of Ma–terials Research and Technology, **25**, 1944–1958 (2023).

[8] Zhang, P.; Lin, Z.; Liu, Z.; Liu, J.; Mai, Q.; Yue, X.: Effect of cutting parameters on the micro–structure evolution and damage mechanism of 7075-T6 aluminum alloy in micro cutting. Inter–national Journal of Damage Mechanics, (2023).

[9] Wan, M.; Ye, X.-Y.; Yang, Y.; Zhang, W.-H.: The–oretical prediction of machining-induced residual stresses in three-dimensional oblique milling pro–cesses. International Journal of Mechanical Scien–ces, **133**, 426–437 (2017).

[10] Yang, D.; Liu, Z.; Ren, X.; Zhuang, P.: Hybrid modeling with finite element and statistical met–hods for residual stress prediction in peripheral mi–lling of titanium alloy Ti-6Al-4V. International Jour–nal of Mechanical Sciences, **108–109**, 29–38 (2016).

[11] Mehner, T.; Junge, T.; Schubert, A., Lampke, T.: Prediction of residual-stress depth profiles in tur–ning of EN AW-2017 based on in-process measu–rements of machining forces and temperatures. IOP Conference Series: Materials Science and Engine–ering. **1147**, 12-19 (2021).

[12] Jacobus, K.; DeVor, R. E.; Kapoor, S. G.; Peascoe, R. A.: Predictive Model for the Full Biaxial Surface and Subsurface Residual Stress Profiles from Turning. Journal of Manufacturing Science and Engineering, **123**, 537–546 (2001).

[13] Denkena, B.; Boehnke, D.; De, L.: Machining induced residual stress in structural aluminum parts. Production Engineering, **2**, 247–253 (2008).

[14] Motorcu, A; Ekici, E.: Evaluation and Multi-Cri–teria Optimization of Surface Roughness, Deviation From Dimensional Accuracy and Roundness Error in Drilling CFRP/Ti6Al4 Stacks. FME Tran–sactions, **50**, 441-460 (2022).

[15] Deepanraj, B.; Raman, L.A; Senthilkumar, N.; Shivasankar, J.: Investigation and Optimization of Machining Parameters Influence on Surface Roug–hness in Turning AISI 4340 Steel. FME Tran–sactions, 48, 383-390 (2020).

[16] Chen, G.; Ge, J.; Lu, L.; Liu, J.; Ren, C.: Mechanism of ultra-high-speed cutting of Ti-6Al-4V alloy considering time-dependent microst–ructure and mechanical behaviors. The International Journal of Advanced Manufacturing Technology. 113, 193-213 (2021).

[17] Abboud, E.; Attia, H.; Shi, B.; Damir, A.; Thom–son, V.; Mebrahtu, Y.: Residual Stresses and Sur–face Integrity of Ti-alloys During Finish Turning – Guidelines for Compressive Residual Stresses. Pro–cedia CIRP, **45**, 55–58 (2016).

[18] Chaize, E.; Dumont, F.; Truffart, B.; Girinon, M.; Brosse, A.; Dorlin, T.; Valiorgue, F.; Rech, J.: Influence of lubrication mode onto residual stress generation in turning. Procedia CIRP, **108**, 390–393 (2022).

[19] Zhang, W.; Wang, X.; Hu, Y.; Wang, S.: Predictive modelling of microstructure changes, micro-hard–ness and residual stress in machining of 304 auste–nitic stainless steel. International Journal of Machi–ne Tools and Manufacture, **130–131**, 36–48 (2018).

[20] Leveille, T.; Valiorgue, F.; Dumas, M.; Masciantonio, U.; Brosse, A.; Karaouni, H.; Rech, J.: 3D numerical modelling of residual stresses induced by reaming. Journal of Manufacturing Processes, **113**, 47–60 (2024).

[21] Tao, L.; Chen, H.; Liu, A.: Finite element analysis of the effect of tool edge radius on residual stresses when orthogonal cutting Ti6Al4V. IOP Conference Series: Materials Science and Engineering, **382**, 042059 (2018).

[22] Lu, Z.; Zhang, D.; Zhang, X.; Peng, Z.: Effects of high-pressure coolant on cutting performance of high-speed ultrasonic vibration cutting titanium alloy. Journal of Materials Processing Technology, **279**, 116584 (2020).

[23] Sarıkaya, M.; Gupta, M. K.; Tomaz, I.; Pimenov, D. Y.; Kuntoğlu, M.; Khanna, N.; Yıldırım, Ç. V.; Krolczyk, G. M.: A state-of-the-art review on tool wear and surface integrity characteristics in machi–ning of superalloys. CIRP Journal of Manufacturing Science and Technology, **35**, 624–658 (2021).

[24] Veeranaath, V.; Das, R. K.; Rai, S. K.; Singh, S.; Sharma, P.: Experimental Study and Optimization of Residual Stresses in Machining of Ti6Al4V Using Titanium and Multi-layered Inserts. IOP Conference Series: Materials Science and Engine–ering, **912**, 032028 (2020).

[25] Outeiro, J.; Cheng, W.; Chinesta, F.; Ammar, A.: Modelling and Optimization of Machining of Ti-6Al-4V Titanium Alloy Using Machine Learning and Design of Experiments Methods. Journal of Manufacturing and Materials Processing, **6**, 58 (2022).

[26] Sahu, N. K.; Andhare, A. B.: Prediction of residual stress using RSM during turning of Ti–6Al–4V with the 3D FEM assist and experiments. SN App–lied Sciences, **1**, 891 (2019).

[27] Abboud, E.; Shi, B.; Attia, H.; Thomson, V.; Mebrahtu, Y.: Finite Element-based Modeling of Machining-induced Residual Stresses in Ti-6Al-4V under Finish Turning Conditions. Procedia CIRP, **8**, 63–68 (2013).

[28] Khandai, D. K.; Mathew, J.; Kuriachen, B.: FEM modelling of residual stresses of Ti-6Al-4V during micro-turning considering the scale effect. Sādhanā, **47**, 107 (2022).

[29] Ozel, T.; Zeren, E.: Finite Element Modeling of Stresses Induced by High Speed Machining With Round Edge Cutting Tools. In *Manufacturing En–gineering and Materials Handling, Parts A and B*; ASMEDC: Orlando, Florida, USA, (2005); pp. 1279–1287.

[30] Meng, L.; Atli, M.; Khan, A. M.; Su, Y.; Fang, C.; Zhang, H.; He, N.: Prediction of residual stresses generated by machining Ti6Al4V alloy based on the combination of the ALE approach and inden–tation model. Journal of the Brazilian Society of Mechanical Sciences and Engineering, **41**, 471 (2019).

[31] Zhuang, K.; Huang, Y.; Weng, J.; Zhang, D.; Zhou, J.: Numerical investigations on residual stresses in orthogonal cutting of Ti-6A1-4V. Procedia CIRP, **108**, 199–204 (2022).

[32] Liu, Y.; Xu, D.; Agmell, M.; Saoubi, R. M.; Ahadi, A.; Stahl, J.-E.; Zhou, J.: Numerical and experi–mental investigation of tool geometry effect on residual stresses in orthogonal machining of Inconel 718. Simulation Modelling Practice and Theory, **106**, 102187 (2021).

[33] Zou, Z.; Zhang, T.; He, L.; Zhao, X.; Zhou, T.: Hybrid modeling prediction of residual stresses in turned Ti6Al4V considering frictional contact. Journal of Materials Research and Technology, **30**, 4377–4392 (2024).

[34] Mabrouki, T.; Rigal, J.-F.: A contribution to a qualitative understanding of thermo-mechanical effects during chip formation in hard turning. Journal of Materials Processing Technology, **176**, 214–221 (2006).

[35] Xu, X.; Outeiro, J.; Zhang, J.; Xu, B.; Zhao, W.; Astakhov, V.: Machining simulation of Ti6Al4V using coupled Eulerian-Lagrangian approach and a constitutive model considering the state of stress. Simulation Modelling Practice and Theory, **110**, 102312 (2021).

[36] Lee, W.-S.; Lin, C.-F.: High-temperature deformation behaviour of Ti6Al4V alloy evaluated by high strain-rate compression tests. Journal of Materials Processing Technology, **75**, 127–136 (1998).

[37] Xu, X.; Zhang, J.; Outeiro, J.; Xu, B.; Zhao, W.: Multiscale simulation of grain refinement induced by dynamic recrystallization of Ti6Al4V alloy during high speed machining. Journal of Materials Processing Technology, **286**, 116834 (2020).

[38] Mabrouki, T.; Girardin, F.; Asad, M.; Rigal, J.-F.: Numerical and experimental study of dry cutting for an aeronautic aluminium alloy (A2024-T351). International Journal of Machine Tools and Manufacture, **48**, 1187–1197 (2008).

[39] Wang, B.; Liu, Z.: Investigations on the chip formation mechanism and shear localization sensitivity of high-speed machining Ti6Al4V. The International Journal of Advanced Manufacturing Technology, **75**, 1065–1076 (2014).

[40] Sima, M.; Özel, T.: Modified material constitutive models for serrated chip formation simulations and experimental validation in machining of titanium alloy Ti–6Al–4V. International Journal of Machine Tools and Manufacture, **50**, 943–960 (2010).

[41] Zhou, T.; He, L.; Zou, Z.; Du, F.; Wu, J.; Tian, P.: Three-dimensional turning force prediction based on hybrid finite element and predictive machining theory considering edge radius and nose radius. Journal of Manufacturing Processes, **58**, 1304–1317 (2020).

[42] Ekici, E.; Motorcu, A. R.; Uzun, G.: Multi-Objective Optimization of Process Parameters for Drilling FiberMetal Laminate Using a Hybrid GRAP–CA Approach. FME Transactions, **49**, 356-366 (2021).

[43] Jomaa, W.; Songmene, V.; Bocher, P.: An Investigation of Machining-Induced Residual Stresses and Microstructure of Induction-Hardened AISI 4340 Steel. Materials and Manufacturing Processes, **31**, 838–844 (2016).

[44] Jomaa, W.; Songmene, V.; Bocher, P.: Surface Finish and Residual Stresses Induced by Orthogonal Dry Machining of AA7075-T651. Materials, **7**, 1603–1624 (2014).

[45] Sun, S.; Brandt, M.; Dargusch, M. S.: Characteristics of cutting forces and chip formation in machining of titanium alloys. International Journal of Machine Tools and Manufacture, **49**, 561–568 (2009).

[46] Su, G.; Liu, Z.; Li, L.; Wang, B.: Influences of chip serration on micro-topography of machined surface in high-speed cutting. International Journal of Machine Tools and Manufacture, **89**, 202–207 (2015).

[47] Haddag, B.; Yameogo, D.; Nouari, M.; Makich, H.: Multi-Physics Analysis of Machining Ti-6Al-4V Alloy: Experimental Characterization and a New Material Behavior Modeling. Metals, **12**, 581 (2022).

[48] Chen, G.; Ge, J.; Lu, L.; Liu, J.; Ren, C.: Mechanism of ultra-high-speed cutting of Ti-6Al-4V alloy considering time-dependent microstructure and mechanical behaviors. The International Journal of Advanced Manufacturing Technology, **113**, 193–213 (2021).

[49] Wan, Z. P.; Zhu, Y. E.; Liu, H. W.; Tang, Y.: Microstructure evolution of adiabatic shear bands and mechanisms of saw-tooth chip formation in machining Ti6Al4V. Materials Science and Engineering: A, **531**, 155–163 (2012).

[50] Davis, B.; Dabrow, D.; Ifju, P.; Xiao, G.; Liang, S. Y.; Huang, Y.: Study of the Shear Strain and Shear Strain Rate Progression During Titanium Machining. Journal of Manufacturing Science and Engineering, **140**, 051007 (2018).

[51] Cotterell, M.; Byrne, G.: Dynamics of chip formation during orthogonal cutting of titanium alloy Ti–6Al–4V. CIRP Annals, **57**, 93–96 (2008).

[52] Li, A.; Zang, J.; Zhao, J.: Effect of cutting parameters and tool rake angle on the chip formation and adiabatic shear characteristics in machining Ti-6Al-4V titanium alloy. The International Journal of Advanced Manufacturing Technology, **107**, 3077–3091 (2020).

[53] Hua, J.; Shivpuri, R.: Prediction of chip morphology and segmentation during the machining of titanium alloys. Journal of Materials Processing Technology, **150**, 124–133 (2004).

[54] T, M.; T, J.; A, S.; T, L.; Li, L.; Zhao, Y.-X.: Simulation analysis and experimental study of milling surface residual stress of Ti-10V-2Fe-3Al. Journal of Manufacturing Processes, **32**, 530–537 (2018).

[55] Holmberg, J.; Rodríguez Prieto, J. M.; Berglund, J.; Sveboda, A.; Jonsén, P.: Experimental and PFEM-simulations of residual stresses from turning tests of a cylindrical Ti-6Al-4V shaft. Procedia CIRP, **71**, 144–149 (2018).

[56] Sun, J.; Guo, Y. B.: A comprehensive experimental study on surface integrity by end milling Ti–6Al–4V. Journal of Materials Processing Technology, **209**, 4036–4042 (2009).

NOMENCLATURE

Vc	Cutting speed
f	Feed

A	Uncut chip
B	Yield stress
n	Hardening modulus
C	Work-hardening exponent
Tr	Strain-rate sensitivity coefficient
Tm	Room temperature
L	Melting temperature
Gf	Characteristic length
Kc	Fracture energy
D	Fracture toughness
Gs	Stiffness degradation of materials
P	Serration degree
V	Pitch
H	Valley
	Peak

Greek symbols

γ	Rake angle
$\bar{\sigma}$	Flow stress
$\dot{\bar{\varepsilon}}$	Plastic strain
$\dot{\bar{\varepsilon}}_0$	Reference strain rate
$\Delta\varepsilon$	Increment of equivalent plastic strain
ε_f	Fracture strain at failure
$\frac{P}{\bar{\sigma}}$	Hydrostatic pressure to the flow stress
$\bar{\varepsilon}_0$	Initial plastic strain
$\bar{u}$	Equivalent plastic displacement
$\bar{u}_f$	Equivalent plastic displacement at failure
σ_{y0}	Yield stress at the damage initiation
τ	Frictional stress
σ	Normal stress
τy	Yield shear stress
μ	Friction coefficient
□	Shear angle

Abbreviations

FEM	Finite Element Method
FE	Finite Element
J-C	Johnson-Cook
RS	Residual Stress
DOE	Design of Experiments
ALE	Arbitrary Lagrangian and Eulerian
CEL	Coupled Eulerian-Lagrangian

ИСТРАЖИВАЊЕ ОДГОВОРА НА СЕЧЕЊЕ ТОКОМ ОБРАДЕ ВЕЛИКЕ БРЗИНЕ ЛЕГУРЕ Ti6Al4V: АНАЛИЗА КОНАЧНИХ ЕЛЕМЕНАТА

А. Чтиути, А. Оубалоуш, А. Мучтачи

Легура титанијума је један од најчешће коришћених материјала у најсавременијим технолошким секторима као што је ваздухопловство. У овом сектору, значајан део компоненти се добија процесом машинске обраде са малим толеранцијама. Добро је познато да обрада има значајан утицај на интегритет површине, што заузврат утиче на век трајања ових компоненти. Овај рад се бави нумеричким истраживањем утицаја параметара резања, односно брзине резања, дубине резања и нагибног угла, на реакције резања као што су морфологија струготине, силе резања и заостали напон. Модел сечења је симулиран коришћењем Лагранжовог приступа методом коначних елемената. Модел заснован на Јохнсон-Цоок-у имплементиран у АБАКУС/Екплицит се користи за симулацију процеса сувог сечења велике брзине легуре титанијума Ти-6Ал-4В као 2Д ортогоналног сечења. Овај модел је потврђен у односу на експерименталне податке објављене у објављеној литератури. Главни налази су представљени и дискутовани.